Studies of Iridium Nanoparticles Using Density Functional Theory Calculations

Tiffany Pawluk, Yasuhiro Hirata, and Lichang Wang*

Department of Chemistry and Biochemistry, Southern Illinois University, Carbondale, Illinois 62901

Received: June 29, 2005; In Final Form: September 8, 2005

The energetics and the electronic and magnetic properties of iridium nanoparticles in the range of 2−64 atoms were investigated using density functional theory calculations. A variety of different geometric configurations were studied, including planar, three-dimensional, nanowire, and single-walled nanotube. The binding energy per atom increases with size and dimensionality from 2.53 eV/atom for the iridium dimer to 6.09 eV/atom for the 64-atom cluster. The most stable geometry is planar until four atoms are reached and three-dimensional thereafter. The simple cubic structure is the most stable geometric building block until a strikingly large 48-atom cluster, when the most stable geometry transitions to face-centered cubic, as found in the bulk metal. The strong preference for cubic structure among small clusters demonstrates their rigidity. This result indicates that iridium nanoparticles intrinsically do not favor the coalescence process. Nanowires formed from linear atomic chains of up to 4-atom rings were studied, and the wires formed from 4-atom rings were extremely stable. Single-walled nanotubes were also studied. These nanotubes were formed by stacking 5- and 6-atom rings to form a tube. The ring stacking with each atom directly above the previous atom is more stable than if the alternate rings are rotated.

1. Introduction

Precious metal nanoparticles are of great interest because of their potential application in the fields of catalysis, magnetic data storage, and optoelectronics.[1−3] Their magnetic and electronic properties differ significantly from their bulk counterparts.[1,4,5] Their catalytic efficiency is due, in large part, to their high surface area-to-volume ratio. The small size of clusters also causes a greater localization of electrons, often giving them higher magnetic moments than their bulk counterparts.[6] These important properties, as well as the overall stability of the nanoparticles, have been shown to be size and structure dependent.[1,3,4,7−15]

Iridium is primarily known for its catalytic activity, and it has been studied both experimentally[5,15−29,36] and theoretically.[11,14,30−35,37−38] Iridium has been shown to be a very effective catalyst for the dissociative chemisorption of methane.[16−19,30−33] Several studies have proposed a low translational energy pathway for the dissociation of methane using iridium as the metal catalyst.[16−19,32−33]

Precious metal nanoparticles are also an important component of automobile catalytic converters due to their ability to remove pollutants such as NO_x from exhaust. Endou et al.[34] performed density functional theory (DFT) calculations on several different metal clusters, including iridium, to investigate their adsorption toward NO. In this study, the group's calculations were limited to tetrahedral geometry of the metal tetramers, with variation of the position of the NO molecule toward the metal. They found the most stable adsorption state of NO toward any of the precious metal clusters was toward the iridium tetramers. In a later study, Endou et al.[35] expanded their DFT work to include metal pentamers in both square pyramidal and trigonal bipyramidal geometries. They again found that iridium showed the strongest adsorption toward NO for both structural geometries,

leading the group to conclude that regardless of the cluster size or geometry, iridium is the best choice for adsorption of NO.

Another area that iridium shows great promise is in biphasic hydrogenation reactions.[20−23] Iridium has been found to be a recyclable catalyst for the hydrogenation of arenes and ketones. No loss of activity has been seen after recycling, making iridium a very efficient reusable catalyst. Cationic iridium species have also been shown to be effective catalysts for C−H and Si−H bond activation.[24,25] Cho et al.[24] found that the iridium catalysts were far more selective than rhodium toward C−H bond activation in arenes.

Most of the studies discussed to this point investigated adsorption of Ir clusters on surfaces or the catalytic activity of iridium complexes. Little work has focused on how the stability, energetics or reactivity of clusters varies with shape or size. Feng et al.[14] performed theoretical calculations using an effective core potential (10s5p3d/2s1p1d) basis set of Gaussian-94. They investigated the reactivity of iridium clusters from 4 to 10 atoms, comparing different isomers at each cluster size. To study the catalytic activity of clusters, they assessed the reactivity based on the energy difference between the highest occupied molecular orbital and the lowest unoccupied molecular orbital (HOMO−LUMO). They found that the reactivity was not only affected by the size of the cluster, but also the geometry and spin multiplicity. Wang and Ehrlich[15] found that shape and size also affect stability. They investigated planar clusters containing 18 to 39 atoms on Ir(111) using a low-temperature field ion microscope and found that the 19 and 39 atom clusters in hexagonal geometries were the most stable.

Most recently, Bussai et al.[38] studied the structures and binding energies of 4-atom iridium clusters using a scalar-relativistic variant of the linear combination of Gaussian-type orbitals fitting-function density functional method (LCGTO−FF-DF), treating all electrons with the Douglas−Kroll−Hess approach in second order. Their results showed a square planar

---

* To whom correspondence should be addressed. E-mail: lwang@chem.siu.edu. Telephone: (618) 453-6476. Fax: (618) 453-6408.

configuration with eight unpaired electrons as the most stable isomer of Ir_4.

Experimentally, it is possible to synthesize iridium clusters of specific sizes. Watzky and Finke[29] reported the synthesis of iridium clusters of approximately 15, 20, 25, and 30 Å, corresponding to cluster sizes of about 150, 300, 560, and 900 atoms, respectively. These sizes are very close to the "magic-number" cluster sizes that correspond to closed shell configurations. Additionally, Bonet et al.[5] synthesized iridium nanoparticles of approximately 3 nm.

It is important to understand the connection between cluster configuration and stability in order to design more efficient catalysts. To that end, we have investigated a variety of sizes and geometric arrangements in this work using density functional theory calculations. Specifically, we studied iridium clusters consisting of 2 to 64 atoms. The results are presented and discussed in section 3.

2. Method

More than 140 iridium clusters that contain 2 to 64 atoms were studied. For cluster sizes larger than 5 atoms, there are many possible isomers that are energetically possible. We did not intend to study every possible isomer in this research. Rather, we chose possible configurations that are truncated from the iridium bulk, as well as possible stable ones based on our experience of building metal clusters. Once the initial geometries were selected, we allowed them to relax to the stable states without any geometric or symmetry constraint.

The calculations were carried out using DFT encoded in the Vienna ab initio simulation package (VASP).[39−41] The electron−ion interactions were described by ultrasoft pseudopotentials.[42] The exchange and correlation energies were calculated with the Perdew−Wang form of the generalized gradient approximation (GGA).[43] A plane wave basis set was used in our calculations with a cutoff energy of 300 eV. The unit cell was chosen to be at least 5 Å larger than the cluster in every dimension. All the parameters used here were tested for convergence. We note that the DFT code in the VASP is used to describe periodic systems and has been tested to be able to describe other metal clusters successfully.[12,13] One of the reasons the VASP program was chosen is to bridge our current work with the future studies of supported Ir clusters where periodic conditions are used to describe the substrate. The current choice of method will enable us to study the Ir clusters and the cluster−substrate interactions on equal footing.

The binding energy per atom, E_B, is given by

$$E_B = (nE_{Atom} - E_{Cluster})/n$$

where E_{Atom} and $E_{Cluster}$ represent the total energy of a single iridium atom and of the cluster, respectively. E_{Atom} was found to be -1.25 eV. We use n to represent the number of atoms in the cluster. Both the units of E_{Atom} and $E_{Cluster}$ are in eV. As such, the unit of E_B is eV/atom.

The magnetic moment (μ) is calculated by

$$\mu = (m_u - m_d)/n$$

where m_u and m_d are the number of electrons with a majority and a minority spin, respectively. The unit of the magnetic moment is μ_B/atom. The HOMO−LUMO energy gap of the system, E_G, is obtained by the difference between the energies of the lowest unoccupied level and of the highest occupied level. The unit of E_G is eV.

Before presenting the calculated results on various Ir clusters, we compared our calculated results with the available experiments of bulk Ir and the Ir dimer. Our calculated bulk Ir lattice constant is 3.89 Å, which agrees well with the experimental bulk lattice constant of 3.84 Å.[44] The calculated cohesive energy, 7.46 eV/atom, is 7.5% larger than the experimental value of 6.94 eV/atom.[44] Although Ir clusters have shown promising properties as discussed in the previous section, only the Ir dimer has been experimentally studied using a third-law method.[45] The dissociation energy (D_0) of the Ir dimer formed from Ir atoms of atomic electronic configuration of $Ir(5d^86s^1)$ was found to be 4.30 eV ($=2.15$ eV/atom). Our calculated value, 2.53 eV/atom, is 18% larger than the experimental measurement. The discrepancy of the cohesive energy for the Ir dimer may be attributed to large errors in the measurement using the third-law method.[46] Furthermore, no experimental bond length of the Ir dimer is reported. The good agreement between our calculation and the bulk Ir experiment and the previous results for Rh[12] and Pd dimers[13] show that the method is appropriate to describe Ir clusters.

3. Results

3.1. The Most Stable Structures. The relaxed stuctures and calculated properties for the various planar and three-dimensional clusters are summarized in Table 1. For each cluster size, the structures are listed with the planar configurations before three-dimensional, each arranged in decreasing order of stability. We use the designation ^iM_n to distinguish between the various clusters, where M represents the dimensionality, P for planar or T for three-dimensional, n represents the number of atoms in the cluster, and i represents the ith isomer at a given cluster size n. When only one cluster is included at a given size and dimensionality, the superscript i is omitted.

We assessed the stability of clusters based on the binding energy per atom, E_B. Clusters with higher binding energy are more stable. The planar geometry is more stable only for the 4-atom clusters. The most stable geometry is three-dimensional thereafter. This trend is different from that of other platinum group elements (PGEs), except for Ru clusters. The most stable Au structure is planar to a cluster size of 13 atoms,[10] Ru prefers planar only for 4-atom clusters,[8] and Pt, Pd, and Rh are always more stable in the three-dimensional configuration.[11]

For iridium, a square configuration of atoms is an important building block. The square structure, $^1P_4$, with a binding energy of 3.77 eV/atom is more stable than the tetrahedron, $^1T_4$, which has a binding energy of only 3.42 eV/atom. This is contrary to the behavior of Pt, Pd, and Rh, all preferring the tetrahedron structure for 4 atoms. Only Ru is more stable in the square configuration.[8] The square building block increases the stability of three-dimensional clusters. The most stable configuration at any cluster size from 4 to 48 atoms is the structure with the most squares. It is not surprising then that the simple cubic structure, $^1T_8$, is the most important building block for small iridium clusters.

The binding energy of the cube, $^1T_8$, is 4.90 eV/atom. The next most stable 8-atom structure, $^2T_8$, is only 4.68 eV/atom. The cube is also more stable than the larger structures $^2T_9$-$^5T_9$, $^4T_{10}$, $^5T_{10}$, $^3T_{12}$, $^3T_{13}$, and $^4T_{13}$, with binding energies ranging from 4.5 to 4.89 eV/atom. Additionally, when atoms are added to the simple cubic structure, as in 9-, 10-, or 13-atom clusters, the most stable configuration is the one with the fewest edges of the cube disturbed by additional bonds. The 9-atom cluster, $^1T_9$, with a binding energy of 4.90 eV/atom, has only one edge of the cube disturbed by the bonds to the additional atom, whereas

Studies of Iridium Nanoparticles

J. Phys. Chem. B, Vol. 109, No. 44, 2005 **20819**

TABLE 1: Structure, Binding Energy (E_B), HOMO−LUMO Energy Gap (E_G), and Magnetic Moment (μ) of Ir Clusters[a]
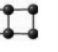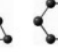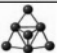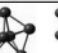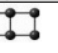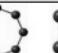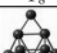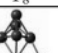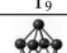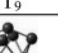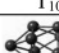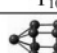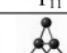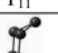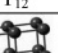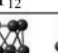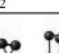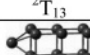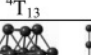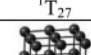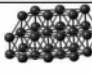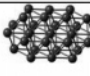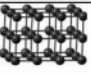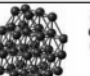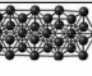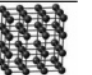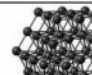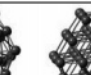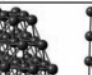
Label (^1M_n)[a]	P_3	$^1P_4$	$^2P_4$	T_4	$^1P_5$	$^2P_5$	$^3P_5$	$^4P_5$
Structure								
Symmetry	C_{2v}	D_{4h}	D_{2h}	C_{1h}	C_{2v}	C_{2v}	C_{2v}	D_{4h}
E_B (eV/atom)	3.03	3.77	3.49	3.42	3.98	3.80	3.75	3.14
E_G (eV)	0.23	0.62	0.07	0.46	0.27	0.31	0.24	0.00
μ (μ_B/atom)	1.00	2.00	1.50	0.00	1.40	1.40	1.00	1.00

Label	$^1T_5$	$^2T_5$	$^3T_5$	$^1P_6$	$^2P_6$	$^3P_6$	$^4P_6$	$^5P_6$
Structure								
Symmetry	D_{4h}	C_{2v}	C_{1h}	C_{2h}	C_{2v}	C_{2v}	D_{2h}	C_{2v}
E_B (eV/atom)	4.01	3.81	3.78	4.26	4.15	4.13	3.70	3.63
E_G (eV)	0.48	0.18	0.11	0.14	0.22	0.30	0.16	0.51
μ (μ_B/atom)	1.40	1.00	1.00	0.67	1.33	1.00	1.00	0.67

Label	$^1T_6$	$^2T_6$	$^3T_6$	$^1P_7$	$^2P_7$	$^1T_7$	$^2T_7$	$^3T_7$
Structure								
Symmetry	C_{1h}	C_{2v}	C_{2v}	D_{2h}	C_{2v}	C_{2v}	C_{2v}	C_1
E_B (eV/atom)	4.38	4.14	3.97	4.03	3.85	4.51	4.45	4.36
E_G (eV)	0.35	0.13	0.25	0.27	0.24	0.29	0.33	0.13
μ (μ_B/atom)	1.33	1.00	1.00	0.71	1.57	1.57	1.00	0.43

Label	$^4T_7$	$^5T_7$	$^6T_7$	$^1P_8$	$^2P_8$	$^1T_8$	$^2T_8$	$^3T_8$
Structure								
Symmetry	C_{1h}	C_{1h}	C_{2v}	D_{2h}	D_{4h}	O_h	D_{2h}	C_1
E_B (eV/atom)	4.35	4.26	4.17	4.35	3.80	4.90	4.68	4.53
E_G (eV)	0.13	0.21	0.24	0.12	0.75	0.33	0.33	0.10
μ (μ_B/atom)	0.14	1.29	0.14	0.25	1.75	0.00	1.25	0.25

Label	$^4T_8$	$^5T_8$	$^6T_8$	$^7T_8$	$^8T_8$	P_9	$^1T_9$	$^2T_9$
Structure								
Symmetry	C_{1h}	C_1	C_{4v}	C_1	D_{2h}	D_{4h}	C_1	C_{1h}
E_B (eV/atom)	4.53	4.52	4.52	4.50	4.50	4.61	4.90	4.87
E_G (eV)	0.16	0.14	0.00	0.21	0.16	0.32	0.17	0.35
μ (μ_B/atom)	0.50	1.50	1.00	0.25	1.00	0.78	0.11	0.11

Label	$^3T_9$	$^4T_9$	$^5T_9$	P_{10}	$^1T_{10}$	$^2T_{10}$	$^3T_{10}$	$^4T_{10}$
Structure								
Symmetry	C_{1h}	C_{4v}	C_{4v}	D_{2h}	C_{2v}	C_{1h}	D_{2h}	C_{4v}
E_B (eV/atom)	4.73	4.65	4.50	4.48	5.02	4.95	4.93	4.85
E_G (eV)	0.19	0.38	0.06	0.14	0.31	0.22	0.13	0.55
μ (μ_B/atom)	0.11	0.55	0.78	0.40	0.40	0.00	0.20	1.40

Label	$^5T_{10}$	$^1T_{11}$	$^2T_{11}$	$^3T_{11}$	$^1T_{12}$	$^2T_{12}$	$^3T_{12}$	$^1T_{13}$
Structure								
Symmetry	C_{4v}	C_{1h}	C_1	C_{1h}	D_{2h}	D_{2h}	C_{1h}	C_{1h}
E_B (eV/atom)	4.76	5.02	5.00	4.96	5.30	4.96	4.89	5.26
E_G (eV)	0.11	0.35	0.38	0.14	0.17	0.27	0.23	0.52
μ (μ_B/atom)	0.60	0.45	0.45	0.09	0.33	0.33	0.67	0.23

Label	$^2T_{13}$	$^3T_{13}$	$^4T_{13}$	P_{16}	$^1T_{18}$	$^2T_{18}$	$^1T_{27}$
Structure							
Symmetry	C_{4v}	C_{2h}	D_{2h}	D_{4h}	D_{2h}	C_1	D_{2h}
E_B (eV/atom)	5.21	4.79	4.74	4.81	5.60	5.32	5.79
E_G (eV)	0.10	0.11	0.23	0.23	0.31	0.10	0.03
μ (μ_B/atom)	0.38	0.54	1.46	0.13	0.33	0.56	0.33

TABLE 1 (Continued)

Label	$^2T_{27}$	$^3T_{27}$	$^1T_{36}$	$^2T_{36}$	$^3T_{36}$	$^1T_{48}$
Structure						
Symmetry	C_1	C_{2h}	D_{2h}	C_1	C_{1h}	D_{2h}
E_B (eV/atom)	5.53	5.39	5.86	5.78	5.56	5.91
E_G (eV)	0.11	0.05	0.18	0.05	0.06	0.01
μ (μ_B/atom)	0.63	0.70	0.31	0.22	0.39	0.00

Label	$^2T_{48}$	$^1T_{55}$	$^2T_{55}$	$^1T_{64}$	$^2T_{64}$
Structure					
Symmetry	C_1	C_1	C_{1h}	C_1	D_{2h}
E_B (eV/atom)	5.91	5.98	5.95	6.09	5.94
E_G (eV)	0.02	0.06	0.10	0.03	0.22
μ (μ_B/atom)	0.15	0.20	0.20	0.19	0.06

[a] The letters P and T represent planar and three-dimensional configurations, respectively. The subscript *n* refers to the number of atoms in the cluster. The superscript *i* distinguishes the *i*th cluster of the designated size *n*, where applicable.
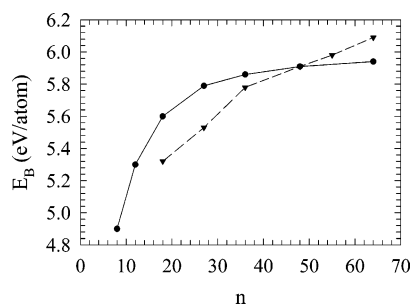
Figure 1. Transition from simple cubic to fcc. The solid and dashed lines represent the binding energy (E_B) in eV/atom of simple cubic structures (●) and those cut from the fcc bulk (▼), respectively, as a function of cluster size, *n*.

$^2T_9$ has 4 edges affected and a lower binding energy of 4.87 eV/atom. This trend also occurs in the 10- and 13-atom clusters. $^1T_{10}$ and $^1T_{13}$ each have only one edge disturbed, while the less stable $^3T_{10}$, $^5T_{10}$ and $^2T_{13}$ have 2, 8, and 4 edges affected by bonds to the additional atoms, respectively. An exception is seen at the 11-atom cluster size. $^3T_{11}$ has only one side disturbed; however the cluster is elongated compared to $^1T_{11}$ and $^2T_{11}$, lowering its stability.

For iridium, the simple cubic structure, $^1T_8$, is more stable than the icosahedron, $^3T_{13}$, or cubooctahedron, $^4T_{13}$, even with 5 fewer atoms. In fact, the structures $^1T_8$, $^2T_9$, $^1T_{10}$, $^3T_{10}$, and $^1T_{12}$, all containing the simple cubic, are all smaller yet more stable than $^3T_{13}$ and $^4T_{13}$. For Pd, the icosahedron, $^3T_{13}$, was found to be the most stable 13-atom cluster, while Pt and Ru prefer the simple cubic based structure, $^2T_{13}$.[11] The binding energy of the icosahedral structure of iridium, $^3T_{13}$, is 4.79 eV/atom. This is higher than the binding energy of 4.43 eV/atom obtained by Yang and Depristo's calculations using the molecular dynamics/Monte Carlo corrected effective medium (MD/MC−CEM) method.[7]

Figure 1 shows the trends in binding energy for simple cubic structures and structures cut from the face-centered cubic (fcc) bulk. The most stable structure is the simple cubic until a remarkable 48-atom cluster size. This further emphasizes the stability of the simple cubic geometry as a building block for larger structures. The transition to fcc bulk structural behavior occurs at a much larger cluster size than is seen for other metals. Only Ru shows a similar trend, with the simple cubic structure the preferred geometry until nearly 40 atoms.[8] The transition occurs near 13 atoms for Pt.[11]
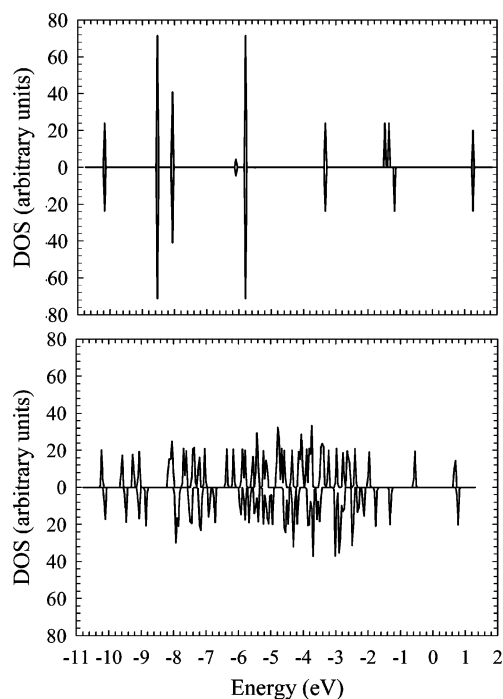
Figure 2. Density of states (DOS) for the cube, $^1T_8$ (top), and the less stable 8-atom structure, $^4T_8$, (bottom). The dashed line represents the Fermi level.

To further investigate the stability of the simple cubic structure, the spin-resolved density of states (DOS) was calculated for the cube, $^1T_8$, and the less stable 8-atom isomer, $^4T_8$. Figure 2 shows the DOS for both of these structures. The DOS for the simple cubic is shown on top. The symmetry of the majority to the minority spin peaks shows good electron pairing consistent with the magnetic moment of zero for the cube. Most of the electron density for $^1T_8$ falls in the lower region of the graph, showing a more inert cluster. The DOS for $^4T_8$ shows poor electron pairing with the majority of the electron density found at higher energy, closer to the Fermi level. The electrons close to the Fermi level are easier to excite, consistent with a more reactive cluster. This supports the data that indicate that the cube is more stable.

Many small metal clusters easily undergo coalescence. One of the factors that influences the coalescence process is the cluster properties. High-resolution electron microscope analysis

Studies of Iridium Nanoparticles

J. Phys. Chem. B, Vol. 109, No. 44, 2005 **20821**
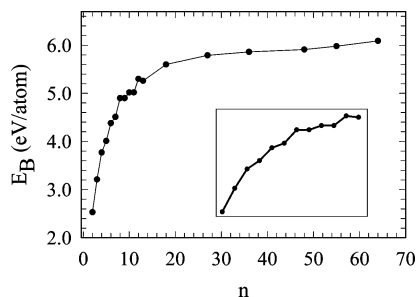
Figure 3. Binding energy, E_B, as a function of cluster size, n. Inset shows expanded region of $n = 2-13$. When more than one isomer is possible, we plot here the most stable one.

Figure 4. HOMO−LUMO energy gap, E_G, as a function of cluster size, n. When more than one isomer is possible, we plot here the most stable one.

Figure 5. Magnetic moment, μ, as a function of cluster size, n. When more than one isomer is possible, we plot here the most stable one.

TABLE 2: Structure and Properties of Iridium Nanowires and Single-Walled Nanotubes

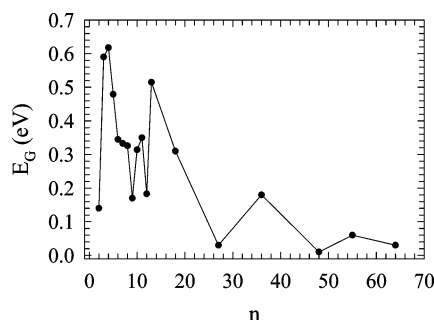| Label Ir_{mxn}[a]	Structure[b]	E_B (eV/atom)	E_G (eV)	μ (μ_B/atom)
Ir_{1x2}		2.53	0.14	2.00
Ir_{1x3}		3.21	0.59	0.33
Ir_{1x4}		3.21	0.34	0.50
Ir_{1x5}		3.34	0.08	1.00
Ir_{1x6}		3.37	0.78	1.33
Ir_{1x7}		3.50	0.46	0.43
Ir_{1x8}		3.51	0.43	0.75
Ir_{1x9}		3.52	0.39	1.00
Ir_{3x2}		4.38	0.34	1.33
Ir_{3x3}		4.75	0.12	0.33
Ir_{3x4}		4.86	0.70	1.00
Ir_{3x5}		4.97	0.35	0.73
Ir_{3x6}		5.04	0.08	0.44
Ir_{3x7}		5.09	0.19	0.52
Ir_{3x8}		5.13	0.32	0.42
Ir_{3x9}		5.15	0.10	0.41
Ir_{3x10}		5.17	0.36	0.47
Ir_{4x2}		4.90	0.32	0.00
Ir_{4x3}		5.30	0.18	0.33
Ir_{4x4}		5.41	0.20	0.25
Ir_{4x5}		5.45	0.18	0.50
Ir_{4x6}		5.56	0.21	0.08
Ir_{4x7}		5.56	0.06	0.29
Ir_{4x8}		5.59	0.08	0.19
Ir_{4x9}		5.63	0.02	0.00
Ir_{5x2}		4.88	0.14	0.40
Ir_{5x3}		5.25	0.07	0.33
Ir_{5x4}		5.35	0.10	0.20
Ir_{5x5}		5.42	0.07	0.28
Ir_{5x6}		5.49	0.02	0.20
Ir_{5x7}		5.51	0.09	0.14
Ir_{5x8}		5.54	0.10	0.05
Ir_{6x2}		4.96	0.24	0.50
Ir_{6x3}		5.32	0.10	0.22
Ir_{6x4}		5.43	0.30	0.42
Ir_{6x5}		5.50	0.14	0.13
Ir_{6x6}		5.56	0.16	0.17
Ir_{6x7}		5.59	0.15	0.19

[a] We use the label $Ir_{m \times n}$ to represent nanowires or nanotubes with m atoms in a single layer and n layers. The label $Ir_{1 \times 6}$ refers to a linear chain of six atoms. The label $Ir_{5 \times 7}$ refers to the structure with seven layers of five-atom rings. [b] Representative structures are each six layers long.

has shown that liquidlike properties of surface atoms play an essential role in this process.[47] The liquidlike property can be related to the similar energetics among isomers with different arrangements of surface atoms. The fluidity characteristic of Pt clusters shown from our previous DFT study[9] indicates that a relatively easy coalescence process will occur among Pt clusters. However, as shown in Table 1, this is not the case for Ir clusters. For instance, to move the top atom of the $^1T_{13}$ cluster to the center to form the configuration $^2T_{13}$, we need to provide at least 0.05 eV of energy, which makes it less liquidlike. This kind of rigidity among small Ir clusters, due to the strong preference for the cubic structure, does not favor the coalescence process.

Figure 3 shows the calculated results for the binding energy of the most stable structure at each cluster size, and it generally increases with cluster size. A staircase is apparent at cluster sizes of 8, 10, and 12 atoms. This is expected because of the increased stability of clusters containing the simple cubic, as was previously discussed.

The HOMO−LUMO energy gap for the most stable geometry at each cluster size is shown in Figure 4. The energy gap decreases oscillatorily with cluster size. Specific values for each geometric configuration are included in Table 1. There is great variation in the energy gap for isomers, showing strong structure dependence for conductivity. For example, the energy gaps for the 4-atom clusters range from 0.07 to 0.62 eV.

For clusters larger than 13 atoms, all are good conductors. This is not surprising, as larger clusters tend toward bulk characteristics. No correlation can be found between the energy gaps and stability, dimensionality, structure, or magnetic moments, aside from the previously mentioned general oscillatory decrease with an increase in cluster size.

Figure 5 shows the trend for the magnetic moments of the most stable structures. As seen in the energy gap, the magnetic moments decrease oscillatorily with increasing cluster size. The magnetic moments do not, however, follow the same pattern
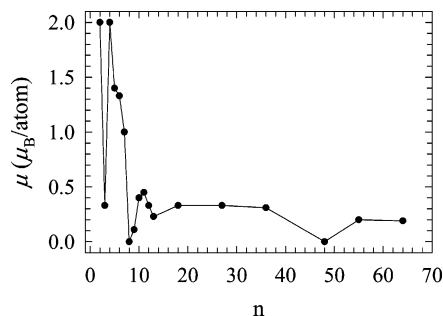
of oscillatory decrease as the energy gaps, allowing no correlation to be drawn.

Many of the smaller clusters exhibit large magnetic moments, with the majority of the clusters from 2 to 8 atoms having magnetic moments larger than 0.5 μ_B/atom, and many above 1.0 μ_B/atom. These substantial magnetic moments are also seen for a few of the larger structures. The clusters $^4T_9$, $^5T_9$, $^3T_{12}$, $^3T_{13}$, $^4T_{13}$, $^2T_{18}$, $^2T_{27}$, and $^3T_{27}$, all exhibit giant magnetic moments larger than 0.5 μ_B/atom.

3.2. Nanowires and Nanotubes. Table 2 shows the results for the nanowires. Included in this category are monatomic linear chains from 2 to 9 atoms long, as well as triatomic and tetra-atomic nanowires formed from stacking triangle or square rings.

20822 *J. Phys. Chem. B, Vol. 109, No. 44, 2005*

Pawluk et al.

These small tubes are considered nanowires because their limited diameter would not allow any material to be placed or synthesized inside the tube, making them functionally nanowires.

Our calculations included linear chains up to 9 atoms long, a length of over 2 nm. The distance between atoms is greater for inner atoms than it is between atoms on the ends of the chain. The interatomic distances alternate symmetrically about the center of the chain, with the average bond distances 2.2−2.3 Å. The stability of the linear chains increases with chain length.

For the triatomic and tetraatomic nanowires, the rings were layered in two ways. The first was so the atoms of each layer aligned along the edges like a linear chain, which we call straight stacking. The second was with a rotation of 60° between the layers of the triangle rings and 45° between the layers of the square rings, which we call twisted stacking. In the case of these ring-based nanowires, the straight stacking was more stable than the twisted configuration.

The triangle ring nanowires were calculated up to 10 layers and were stable up to this length, about 2.5 nm. The average interlayer distances were 2.3−2.5 Å. The interlayer distances compacted slightly in the middle of the wires, and also compacted on the ends of the longer wires, over 6 layers long. The square ring wires were stable up to 9 layers, about 2.2 nm. The average interlayer distances were 2.4−2.5 Å, with a similar pattern of contraction in the middle and on the ends of longer wires. The diameters of the rings were slightly smaller in the rings toward the center of the wires for both triatomic and tetraatomic wires. Our results showed all of these nanowires maintained structural integrity, holding in the shape of a nanowire without any significant bending or twisting.

Single-walled nanotubes (SWNTs) were formed from stacking 5- or 6-atom rings in the straight and twisted layering patterns described above. For the twisted tubes, the pentagon rings were rotated 36° between layers, and the hexagons were rotated 30°. The results of these calculations are also included in Table 2. As seen with the nanowires, the straight layering method results in a more stable SWNT in every case.

The pentagon tubes were extended to 8 layers, about 2 nm, before a loss of structural integrity. The interlayer distances varied from 2.4 to 2.6 Å, with the longer distances falling in the center of the tube, unlike the tri- and tetraatomic wires. The hexagon tubes were only stable up to 7 layers, about 1.5 nm long. The interlayer distances were 2.3−2.5 Å, again with the longer distances between central layers. A slight translational shift is seen in the layers of the pentagon tubes longer than 6 layers and hexagon tubes longer than 4 layers. The tube diameters are slightly larger in the center of the tube layers for both the pentagon and hexagon tubes.

Figure 6 shows the binding energy for the nanowires and nanotubes as a function of the total number of atoms in each structure. The nanowires formed from the square rings are substantially more stable than those formed from the triangle rings. This is due to the added stability of the simple cubic structure. Each additional square layer that is added to the wire results in the formation of another cube. It is therefore not surprising that this configuration would be very stable. The wires formed from square rings are also more stable than tubes formed from 5- and 6-atom rings.

Figure 7 shows the binding energy as a function of the total number of layers for the wires and tubes. The nanowires formed with 6-atom rings are the most stable for any number of layers, not surprising since each hexagon layer has the most atoms. However, the nanowires with stacked squares are almost as
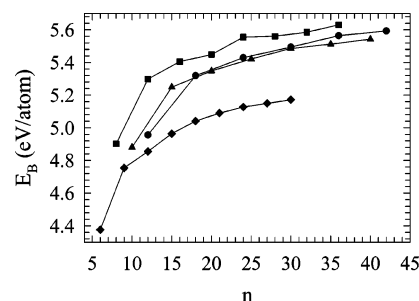

Figure 6. Nanowire and nanotube binding energy, E_B, as a function of cluster size, n. The binding energy for nanowires and nanotubes formed from stacked rings of triangles (◆), squares (■), pentagons (▲), and hexagons (●), as a function of cluster size.
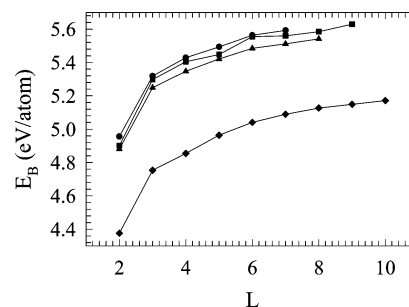

Figure 7. Binding energy, E_B, as a function of the number of layers, L, in each tube. The binding energy for nanowires and nanotubes formed from stacked rings of triangles (◆), squares (■), pentagons (▲), and hexagons (●), as a function of the number of layers of stacked rings.

stable, even though each layer contains 2 fewer atoms. This further supports our findings that the square is a stabilizing element in the buildup of clusters.

4. Conclusions

The energetic, electronic, and magnetic properties of iridium nanoparticles from 2 to 64 atoms were investigated using DFT calculations. The binding energy, HOMO−LUMO energy gap, and magnetic moment were calculated and discussed to gain a better understanding of the link between structure and these properties. The stability of the clusters increases with cluster size. The HOMO−LUMO energy gap and magnetic moment both decrease oscillatorily with increasing cluster size. Most of the clusters studied exhibit good conductor behavior, and many have giant magnetic moments.

The simple cubic structure was found to be a most important building block for clusters of iridium nanoparticles. Clusters with this geometric feature are more stable than clusters of corresponding size lacking the cube. The simple cubic geometries are more stable until a strikingly large cluster size of 48 atoms, when the most stable geometry transitions to fcc. The strong preference for forming cubic structures among small iridium clusters indicates that these nanoparticles are very resistant to coalescence compared to other metals clusters, such as Pd and Pt.

Nanowires formed from linear atomic chains of single atoms and 3- and 4-atom rings were also investigated. The added stability of the simple cubic geometry is further seen in the nanowires created by stacking 4-atom rings to form linear chains. These nanowires are extremely stable for their size, and very stable compared to larger nanotubes.

Calculations were also performed on single walled nanotubes (SWNTs) formed from stacking pentagons and hexagons to form tubes. The pentagon tubes were stable up to about 2 nm long, while the hexagon tubes were only stable until 1.5 nm. Stacking

Studies of Iridium Nanoparticles

J. Phys. Chem. B, Vol. 109, No. 44, 2005 **20823**

the subsequent layers without any rotation of the rings resulted in the most stable SWNTs.

References and Notes

(1) Eberhardt, W. *Surf. Sci.* **2002**, *500*, 242.

(2) Yee, C. K.; Jordan, R.; Ulman, A.; White, H.; King, A.; Rafailovich, M.; Sokolov, J. *Langmuir* **1999**, *15*, 3486.

(3) Yang, L.; DePristo, A. E. *J. Catal.* **1994**, *149*, 223.

(4) Yang, S. H.; Drabold, D. A.; Adams, J. B.; Ordejon, P.; Glassford, K. *J. Phys.: Condens. Matter* **1997**, *9*, L39.

(5) Bonet, F.; Delmas, V.; Grugeon, S.; Herrera Urbina, R.; Silvert, P.-y.; Tekaia-Elhsissen, K. *Nanostructured Mater.* **1999**, *11*, 1277.

(6) Gantefor, G.; Eberhardt, W. *Phys. Rev. Lett.* **1996**, *76*, 4975.

(7) Yang, L.; DePristo, A. E. *J. Chem. Phys.* **1994**, *100*, 725.

(8) Zhang, W.; Zhao, H.; Wang, L. *J. Phys. Chem. B* **2004**, *108*, 2140.

(9) Xiao, L.; Wang, L. *J. Phys. Chem. A* **2004**, *108*, 8605.

(10) Xiao, L.; Wang, L. *Chem. Phys. Lett.* **2004**, *392*, 452.

(11) Zhang, W.; Xiao, L.; Hirata, Y.; Pawluk, T.; Wang, L. *Chem. Phys. Lett.* **2004**, *383*, 67.

(12) Wang, L.; Ge, Q. *Chem. Phys. Lett.* **2002**, *366*, 368.

(13) Zhang, W.; Ge, Q.; Wang, L. *J. Chem. Phys.* **2003**, *118*, 5793.

(14) Feng, J.-N.; Huang, X.-R.; Li, Z.-S. *Chem. Phys. Lett.* **1997**, *276*, 334.

(15) Wang, S. C.; Ehrlich, G. *Surf. Sci.* **1997**, *391*, 89.

(16) Reeves, C. T.; Seets, D. C.; Mullins, C. B. *J. Mol. Catal. A: Chem.* **2001**, *167*, 207.

(17) Seets, D. C.; Wheeler, M. C.; Mullins, C. B. *Chem. Phys. Lett.* **1997**, *266*, 431.

(18) Seets, D. C.; Wheeler, M. C.; Mullins, C. B. *J. Chem. Phys.* **1997**, *107*, 3986.

(19) Seets, D. C.; Reeves, C. T.; Ferguson, B. A.; Wheeler, M. C.; Mullins, C. B. *J. Chem. Phys.* **1997**, *107*, 10229.

(20) Dupont, J.; Fonseca, G. S.; Umpierre, A. P.; Fichtner, P. F. P.; Teixeira, S. R. *J. Am. Chem. Soc.* **2002**, *124*, 4228.

(21) Fonseca, G. S.; Umpierre, A. P.; Fichtner, P. F. P.; Teixeira, S. R.; Dupont, J. *Chem.—Eur. J.* **2003**, *9*, 3263.

(22) Fonseca, G. S.; Scholten, J. D.; Dupont, J. *Synth. Lett.* **2004**, *9*, 1525.

(23) Mevellec, V.; Roucoux, A.; Ramirez, E.; Philippot, K.; Chaudret, B. *Adv. Synth. Catal.* **2004**, *346*, 72.

(24) Cho, J.-Y.; Tse, M. K.; Holmes, D.; Maleczka, R. E., Jr.; Smith, M. R., III. *Science* **2002**, *295*, 305.

(25) Klei, S. R.; Tilley, T. D.; Bergman, R. G. *J. Am. Chem. Soc.* **2000**, *122*, 1816.

(26) Lai, F. S.; Gates, B. C. *Nano Lett.* **2001**, *1*, 583.

(27) Hyaek, K.; Goller, H.; Penner, S.; Rupprechter, G.; Zimmermann, C. *Catal. Lett.* **2004**, *92*, 1.

(28) Berko, A.; Solymosi, F. *Surf. Sci. Lett.* **1998**, *411*, L900.

(29) Watzky, M. A.; Finke, R. G. *Chem. Mater.* **1997**, *9*, 3083.

(30) Liao, M.-S.; Zhang, Q.-E. *J. Mol. Catal. A: Chem.* **1998**, *136*, 185.

(31) Au, C.-T.; Ng, C.-F.; Liao, M.-S. *J. Catal.* **1999**, *185*, 12.

(32) Sitz, G. O.; Mullins, C. B. *J. Phys. Chem. B* **2002**, *106*, 8349.

(33) Strout, D. L.; Zaric, S.; Niu, S.; Hall, M. B. *J. Am. Chem. Soc.* **1996**, *118*, 6068.

(34) Endou, A.; Ohashi, N.; Yoshizawa, K.; Takami, S.; Kubo, M.; Miyamoto, A.; Broclawik, E. *J. Chem. Phys. B* **2000**, *104*, 5110.

(35) Endou, A.; Jung, C.; Kusagaya, T.; Kubo, M.; Selvam, P.; Miyamoto, A.; *Appl. Surf. Sci.* **2004**, *223*, 159.

(36) Ferrari, A. M.; Neyman, K. M.; Mayer, M.; Staufer, M.; Gates, B. C.; Rosch, N. *J. Phys. Chem. B* **1999**, *103*, 5311.

(37) Jimenez-Catano, R.; Niu, S.; Hall, M. B. *Organometallics* **1997**, *16*, 1962.

(38) Bussai, C.; Krüger, S.; Vayssilov, G.; Rösch, N. *Phys. Chem. Chem. Phys.* **2005**, *13*, 2656.

(39) Kresse, G.; Hafner, J. *Phys. Rev. B* **1993**, *47*, 558.

(40) Kresse, G.; Furthmuller, J. *Phys. Rev. B* **1996**, *54*, 11169.

(41) Kresse, G.; Furthmuller, J. *Comput. Mater. Sci.* **1996**, *6*, 15.

(42) Vanderbilt, D. *Phys. Rev. B* **1990**, *41*, 7892.

(43) Perdew, J. P.; Chevary, J. A.; Vosko, S. H.; Jackson, K. A.; Pederson, M. R.; Singh, D. J.; Fiolhais, C. *Phys. Rev. B* **1992**, *46*, 6671.

(44) Kittel, C. *Introduction to Solid-State Physics, 5th ed.* Wiley: New York, 1976.

(45) Miedema, A. R.; Gingerich, K. A. *J. Phys. B: At. Mol. Phys.* **1979**, *12*, 2081.

(46) Lombardi, J. R,; Davis, B. *Chem. Rev.* **2002**, *102*, 2431.

(47) Jose-Yacaman, M.; Gutierrez-Wing, C.; Miki, M.; Ynag, D.-Q.; Piyakis, K. N.; Sacher, J. *J. Phys. Chem. B* **2005**, *109*, 9703.